ciation reactions of relatively complex biomolecules. In addition, detailed questions on the factors which govern the dissociation chemistry of these systems can be obtained by appropriate choice and positioning of the chromophoric group.

Acknowledgment. This work was supported by grants from the U.S. Department of Energy, Division of Chemical Sciences, Office of Basic Energy Sciences (DE-AS05-82ER13023), and the National Science Foundation (CHE-8418457).

Registry No. DNP-Gly-OH, 1084-76-0; DNP-Ala-OH, 1655-52-3; DNP-β-Ala-OH, 3185-97-5; DNP-Val-OH, 1694-97-9; DNP-Leu-OH, 1655-57-8; DNP-Ile-OH, 1655-56-7; DNP-His-OH, 10457-26-8; DNP-Phe-OH, 1655-54-5; DNP-Trp-OH, 1655-51-2; DNP-Gly-Ala-OH, 58979-22-9; DNP-Gly-β-Ala-OH, 118439-08-0; DNP-Gly-Val-OH, 58979-23-0; DNP-Pro-Leu-Gly-OH, 65985-66-2; DNP-Pro-Gln-Gly-OH, 65080-33-3.

Tunneling in Spin-State Interconversion of Ferrous Spin-Crossover Complexes: Concentration Dependence of Apparent Activation Energy Determined in Solution by Laser-Flash Photolysis

Andrew J. Conti, Chuan-Liang Xie, and David N. Hendrickson*

Contribution from the School of Chemical Sciences, University of Illinois, Urbana, Illinois 61801. *Received June 21, 1988*

Abstract: The pulsed-laser photolysis technique is used to monitor the relaxation from the high-spin state ($^5T_2$) to the low-spin ground state ($^1A_1$) of a series of Fe^{II} spin-crossover complexes. The hexadentate ligand is the Schiff base condensate from the reaction of x moles of 6-methyl-2-pyridinecarboxaldehyde, y moles of 2-pyridinecarboxaldehyde, and 1 mole of tris(2-aminoethyl)amine (tren), which gives complexes of the composition $[Fe(6\text{-Me-py})_x(py)_y tren](ClO_4)_2$. Complex **1** ($x = 3, y = 0$) is high-spin in acetone at room temperature, complex **4** ($x = 0, y = 3$) is low-spin, and complexes **2** ($x = 2, y = 1$) and **3** ($x = 1, y = 2$) have both high- and low-spin complexes in equilibrium in acetone at room temperature. At $\sim 5 \times 10^{-4}$ M in acetone, the complexes **2**, **3**, and **4** give $^5T_2 \rightarrow {}^1A_1$ relaxation rate constants (k), which for each complex in the range of 180–300 K give linear ln k versus $1/T$ plots. Apparent Arrhenius activation energies (slopes of the line) are found to be 1029 (19) cm^{-1} for **2**, 870 (15) cm^{-1} for **3**, and 648 (12) cm^{-1} for **4**. Variable-temperature relaxation data are also presented for complex **2** at $\sim 5 \times 10^{-4}$ M in acetonitrile, dichloromethane, methanol, and (2:1) toluene/acetonitrile. The apparent activation energy for complex **2** is found to be solvent dependent with values of 1310 (34) cm^{-1} for acetonitrile, 1170 (23) cm^{-1} for dichloromethane, 1080 (24) cm^{-1} for methanol, and 1010 (20) cm^{-1} for (2:1) toluene/acetonitrile. In an effort to understand the factors determining these energies the concentration dependence of the activation energy for complex **4** was determined from 0.0539 to 0.500 mM in acetone. The activation energy for the $^5T_2 \rightarrow {}^1A_1$ conversion decreases linearly with increasing concentration from 1072 (28) cm^{-1} at 0.0539 mM to 649 (12) cm^{-1} at 0.500 mM. Electrical conductivity measurements for complexes **2**, **3**, and **4** in acetone show that the level of ion pairing (aggregation) is changing throughout the ~0.05 to 0.5 mM range. Fitting of the relaxation data to Hopfield's theoretical model for tunneling between two weakly interacting states indicates that ion pairing affects the zero-point energy difference (ΔE_0) between the $^5T_2$ and $^1A_1$ states. As the concentration of complex **4** in acetone is increased, ΔE_0 increases. The tunneling rate for the complex converting from a given vibrational level of the $^5T_2$ state to a vibrational level which is of similar energy in the $^1A_1$ potential well increases as ΔE_0 increases.

In a recent paper[1] the pulsed-laser photolysis technique was employed to monitor in the 300 to 4.2 K range the relaxation rate from the high-spin state ($^5T_2$) to the low-spin state ($^1A_1$) of a Fe^{II} spin-crossover complex doped in polystyrene sulfonate. It was found that at temperatures below ~120 K the relaxation rate becomes relatively independent of temperature with a value of 1.4 (±0.5) × 10^4 s^{-1} in the 50–4.2 K range. This lack of temperature dependence of the rate is direct evidence that the Fe^{II} complex quantum mechanically tunnels from the $^1A_1$ to the $^5T_2$ state in the low-temperature region. Furthermore, all of the relaxation data in the 300–4.2 K range were fit to two different theoretical models for tunneling between two states. It was shown that a Boltzmann population of vibrational levels of the $^5T_2$ state, where the tunneling rate increases with an increase in vibrational quantum number, could account for an increase in the relaxation rate to 2.33 × 10^7 s^{-1} at 300 K. Thus, it was concluded[1] that the Fe^{II} complex was not necessarily thermally activated over a potential-energy barrier, but the Arrhenius-like behavior of the relaxation rate above ~150 K could be due to tunneling.

Several groups have investigated the spin-state interconversion phenomenon in solution using either the laser Raman[2] or ultrasonic absorption[3] temperature-jump techniques. Among other conclusions, it was found that spin-state interconversions occur faster in solution than in the solid state and that there was no concentration dependence of the kinetics.

McGarvey and co-workers[4] were the first to use the pulsed-laser photolysis technique to determine spin-state relaxation rates for spin-crossover complexes in solution. The pulsed-laser photolysis technique gives better precision in determining these rates than do the temperature-jump techniques. McGarvey et al.[4] were also able to study spin-crossover complexes in solution over a larger

(1) Xie, C.-L.; Hendrickson, D. *J. Am. Chem. Soc.* **1987**, *109*, 6981–6988.

(2) (a) Beattie, J. K.; Sutin, N.; Turner, D. H.; Flynn, G. W. *J. Am. Chem. Soc.* **1973**, *95*, 2052. (b) Dose, E. V.; Tweedle, M. F.; Wilson, L. J.; Sutin, N. *Ibid.* **1977**, *99*, 3886. (c) Hoselton, M. A.; Drago, R. S.; Wilson, L. J.; Sutin, N. *Ibid.* **1976**, *98*, 6967. (d) Petty, R. H.; Dose, E. V.; Tweedle, M. F.; Wilson, L. J. *Inorg. Chem.* **1978**, *17*, 1064. (e) Dose, E. V.; Murphy, K. M.; Wilson, L. J. *Ibid.* **1976**, *15*, 2622. (f) Reeder, K. A.; Dose, E. V.; Wilson, L. J. *Ibid.* **1978**, *17*, 1071. (g) Dose, E. V.; Hoselton, M. A.; Sutin, N.; Tweedle, M. F.; Wilson, L. J. *J. Am. Chem. Soc.* **1978**, *100*, 1142.

(3) (a) Beattie, J. K.; Binstead, R. A.; West, R. J. *J. Am. Chem. Soc.* **1978**, *100*, 3044. (b) Binstead, R. A.; Beattie, J. K.; Dewey, T. G.; Turner, D. H. *Ibid.* **1980**, *102*, 6442.

(4) (a) Lawthers, I.; McGarvey, J. I. *J. Am. Chem. Soc.* **1984**, *106*, 4280. (b) McGarvey, J. I.; Lawthers, I.; Toftlund, H. *J. Chem. Soc., Chem. Commun.* **1984**, 1576. (c) McGarvey, J. J.; Lawthers, I. *Ibid.* **1982**, 906.

0002-7863/89/1511-1171$01.50/0

temperature range. Activation parameters were evaluated; however, McGarvey et al.[4] also reported that there was no concentration dependence.

In light of the recent observation[5] that the energy, line width, and oscillator strength of the intervalence-transfer (IT) electronic absorption band for the mixed-valence biferrocenium cation were found to be concentration dependent, a study of the concentration dependence of the spin-state relaxation rate for spin-crossover complexes in solution was initiated. The quantum mechanics for a binuclear mixed-valence complex and for a spin-crossover complex are analogous. In each case two vibronic states interact to give a ground-state potential-energy surface with two minima separated by a barrier. The magnitude of the zero-point energy difference between the two minima is expected to affect the rate of tunneling of a given complex between the two minima (states). In low- or medium-dielectric solvents these cationic complexes could well be ion paired (or higher aggregates) and if the degree of ion pairing changes with concentration, this should change the zero-point energy difference between the two minima on the ground-state surface. In this paper we show some surprisingly large changes in apparent Arrhenius activation energy as a function of the concentration of a spin-crossover complex in solution.

Experimental Section

Compound Preparation. Elemental analyses were performed in the Microanalytical Laboratory of the School of Chemical Sciences. Commercially available tris(2-aminoethyl)amine, i.e., tren (98% pure, Aldrich), was purified by converting it to its hydrochloride salt, followed by recrystallization in ethanol solution. Anal. Calcd for N-$(CH_2CH_2NH_2)_3$·3HCl: C, 28.20; H, 8.28; N, 21.91. Found: C, 28.30; H, 8.28; N, 21.88. Other commercially available reagents were used without further purification. Samples of the four Fe^{II} complexes studied in this work were prepared by a modification of the method reported by Hoselton et al.[6] All syntheses were carried out under an argon atmosphere employing Schlenkware.

[Fe(6-Me-py)$_3$tren](ClO$_4$)$_2$ (1). To 60 mL of absolute methanol were added 0.542 g (2 mmol) of tren·3HCl and 0.726 g (6 mmol) of 6-methyl-2-pyridinecarboxyaldehyde (Aldrich); 0.34 g of NaOMe was introduced to deprotonate the tren·3HCl. The yellow-orange colored Schiff base solution was then degassed and transferred into the flask which contained a solution of 0.40 g (2 mmol) of $FeCl_2·4H_2O$ in 30 mL of methanol under Ar. The solution color changed from yellow-orange to dark red. To this solution was added 1.3 g of $NaClO_4$ in a small amount of methanol. A microcrystalline product immediately formed and was filtered and washed successively with oxygen-free methanol and ether. The product was then dried in an Ar stream. Anal. Calcd for $FeC_{27}H_{33}N_7O_8Cl_2$: C, 45.65; H, 4.68; N, 13.79; Fe, 7.87. Found: C, 44.82; H, 4.66; N, 13.43; Fe, 7.93.

[Fe(6-Me-py)$_2$(py)tren](ClO$_4$)$_2$ (2). The preparation of complex **2** is the same as for complex **1**, except the Schiff-base solution was made by first dissolving 0.542 g (2 mmol) of tren·HCl in 60 mL of absolute methanol containing 0.34 g of NaOMe and, then, adding 0.484 g (4 mmol) of 6-methyl-2-pyridinecarboxaldehyde followed after 30 min by 0.214 g (2 mmol) of 2-pyridinecarboxaldehyde. Anal. Calcd for $FeC_{26}H_{31}N_7O_8Cl_2$: C, 44.85; H, 4.49; N, 14.07; Fe, 8.02. Found: C, 43.93; H 4.51; N, 13.74; Fe, 8.18.

[Fe(6-Me-py)(py)$_2$tren](ClO$_4$)$_2$ (3). The preparation of complex **3** was the same as for complex **2**, except 2-pyridinecarboxaldehyde and 6-methyl-2-pyridinecarboxaldehyde were used in the ratio of 2:1, respectively, instead of the 1:2 ratio used for complex **2**. Anal. Calcd for $FeC_{25}H_{29}N_7O_8Cl_2$: C, 44.01; H, 4.28; N, 14.36; Fe, 8.19. Found: C, 43.16; H, 4.36; N, 14.11; Fe, 8.12.

[Fe(py)$_3$tren](ClO$_4$)$_2$ (4). The preparation of complex **4** was the same as for complex **1** except 0.642 g (6 mmol) of 2-pyridinecarboxaldehyde was used instead of the 6-methyl-2-pyridinecarboxaldehyde. Anal. Calcd for $FeC_{24}H_{27}N_7O_8Cl_2$: C, 43.14; H, 4.07; N, 14.67; Fe, 8.35. Found: C, 42.75; H, 4.05; N, 14.59; Fe, 8.32.

Physical Measurements. ^{57}Fe Mössbauer spectra were run on a constant-acceleration spectrometer which was described previously.[7] The estimated accuracy of absolute sample temperature determination is ±1 K below 10 K, better than ±2 K for the 20–30 K region, and ±3 K for temperatures above ~30 K. The relative precision of temperature determination is ±0.5 K at the higher temperatures. Isomer shift data are reported relative to iron foil at 298 K, but isomer shifts are not corrected for second-order Doppler effects. It should be noted that isomer shifts illustrated in the figures are displaced slightly from the actual values, whereas accurate values are to be found in the tabulated results. Computer fittings of the Mössbauer data to Lorentzian line shapes were carried out with a modified version of a previously reported computer program.[8]

Variable-temperature magnetic data were collected on a VTS-50 Series 800 SQUID susceptometer (S.H.E. Corp.) interfaced with an Apple IIe personal computer. The sample was tightly packed in a cylindrically shaped Delrin sample container with an inner diameter of about 4 mm. Sample temperature control was achieved by means of a S.H.E. digital temperature monitor. Each data point was taken by averaging 10 measurements taken after the sample reached temperature equilibrium. Pascal constants were employed for the value of the diamagnetic susceptibility.

Variable-temperature UV–vis electronic absorption spectra were recorded on a Varian Model 2300 UV–vis–NIR spectrophotometer with a Janis optical dewar. The optical windows of the dewar consisted of $^1/_8$-in. fused silica and quartz plates, and they were carefully balanced by two other quartz plates in the reference beam. An L-shaped metal sample holder was used to hold the optical cell. The sample holder was attached to the tip of the shaft which came with the dewar. The metal sample holder provided sufficient heat conduction. The temperature sensor and heater were located on the tip of the shaft. A Lake Shore Cryotronics Model DST-80D temperature controller was used to control the sample temperature. Before each spectrum was taken, a period of 20 min was allowed for the sample to reach temperature equilibrium. The spectrum recorded at room temperature with a blank solution was subtracted from each spectrum as a baseline correction. A slight baseline shift was observed as the temperature was decreased, and this shift was compensated by means of a zero-point correction, which brought the absorbance of each spectrum to zero at 800 nm.

The pulsed-laser photolysis experiments were carried out with a Q-switched Molectron Nd/YAG pulsed laser at a frequency doubling mode of 532 nm with a pulse width of 35 ns and about 150 mJ per pulse power output. The probe beam pathway consisted of a xenon flash lamp, an optical lens, a sample holder, a monochromator, and a photomultiplier tube. The Nd/YAG laser and the data acquisition system were synchronized by a timing box. A Tektronix R7912 transient digitizer and a Tektronix computer were used for data acquisition and storage. Each time-resolved electronic absorption profile consisted of 512 sampling points. Each profile was stored on floppy disk and transferred to a VAX 11-780 computer for analysis. Control of the sample temperature was effected with a Janis optical dewar combined with a Lake Shore Cryotronics Model DST-80D temperature controller. Before each spectrum was recorded in the relaxation studies, the sample was allowed to reach temperature equilibrium for a period of 20 min.

Results and Discussion

Properties of Solid-State Spin-Crossover Complexes. The following four Fe^{II} complexes, all as ClO_4^- salts, were studied in this work:

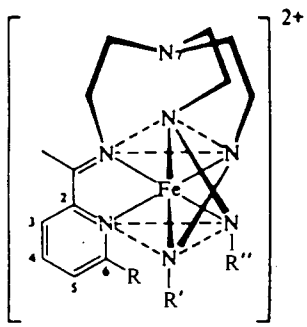

In the case of complex **1**, [Fe(6-Me-py)$_3$tren](ClO$_4$)$_2$, R = CH_3 and R′ and R″ are the same 6-methyl-2-pyridinecarboxaldehyde Schiff-base arms as explicitly indicated for the R-substituted arm. Complex **2** has two 6-methyl-substituted and one unsubstituted pyridine arm; complex **3** has two unsubstituted and one 6-

(5) Lowery, M. D.; Hammack, W. S.; Drickamer, H. G.; Hendrickson, D. N. *J. Am. Chem. Soc.* **1987**, *109*, 8019.
(6) Hoselton, M. A.; Wilson, L. J.; Drago, R. S. *J. Am. Chem. Soc.* **1975**, *97*, 1723.
(7) Cohn, M. J.; Timken, M. D.; Hendrickson, D. N. *J. Am. Chem. Soc.* **1984**, *106*, 6683.
(8) Chrisman, B. L.; Tumolillo, T. A. *Comput. Phys. Commun.* **1971**, *2*, 322.

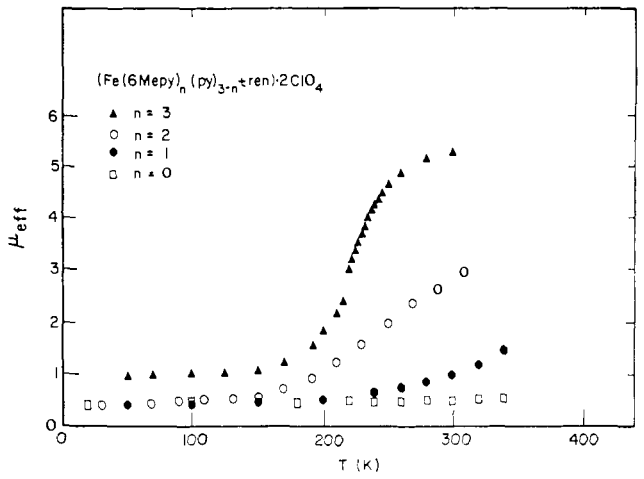

Figure 1. Plots of effective magnetic moment per iron ion, μ_{eff}/Fe, versus temperature for (▲) [Fe(6-Me-py)$_3$tren](ClO$_4$)$_2$ (**1**), (○) [Fe(6-Me-py)$_2$(py)tren](ClO$_4$)$_2$ (**2**), (●) [Fe(6-Me-py)(py)$_2$tren](ClO$_4$)$_2$ (**3**), and (□) [Fe(py)$_3$tren](ClO$_4$)$_2$ (**4**).

Table I. Mössbauer Least-Squares Fitting Parameters for [Fe(6-Me-py)$_3$tren](ClO$_4$)$_2$ (**1**)

T (K)	δ (mm/s)[a]	ΔE_Q (mm/s)[b]	$\Gamma_{1/2}(-)$[c]	$\Gamma_{1/2}(+)$[d]	f_{HS}[d]
320	0.907 (12)	1.375 (1)	0.171 (2)	0.172 (2)	0.75
	0.277 (1)	0.942 (1)	0.239 (1)	0.265 (1)	
300	0.031 (1)	1.369 (1)	0.187 (1)	0.201 (1)	0.76
	0.307 (2)	0.921 (3)	0.203 (2)	0.243 (2)	
270	0.955 (1)	1.487 (1)	0.194 (1)	0.217 (2)	0.72
	0.324 (2)	0.853 (2)	0.321 (2)	0.268 (3)	
255	0.970 (2)	1.542 (1)	0.219 (1)	0.204 (2)	0.62
	0.323 (1)	0.605 (1)	0.352 (3)	0.318 (2)	
240	1.007 (2)	1.557 (2)	0.213 (1)	0.189 (1)	0.50
	0.311 (2)	0.392 (1)	0.228 (2)	0.340 (2)	
210	0.888 (1)	1.970 (3)	0.147 (3)	0.221 (5)	0.10
	0.347 (1)	0.324 (2)	0.237 (1)	0.189 (1)	
180	0.345 (2)	0.335 (1)	0.149 (1)	0.172 (2)	0.0
100	0.342 (1)	0.335 (2)	0.136 (1)	0.170 (1)	0.0
30	0.337 (1)	0.336 (1)	0.124 (1)	0.168 (1)	0.0

[a] Center shift relative to iron foil at 300 K. [b] Quadrupole splitting. [c] Half-width at half-height for the left-side peak of a doublet. [d] Half-width at half-height for the right-side peak of a doublet. [e] High-spin fraction estimated from the absorption area ratio.

methyl-substituted arms; and complex **4** has all three arms with unsubstituted pyridine moieties.

In order to interpret the results of the laser-flash photolysis studies for these four complexes in solution, it was important to know how the spin-state distribution varies in the above four complexes. This information is most easily obtained from solid-state variable-temperature magnetic susceptibility data. Illustrated in Figure 1 is a plot of μ_{eff} versus temperature for each of these complexes. It can be seen that complex **4** remains low spin up to 340 K. Complexes **2** and **3** develop small high-spin populations, 26 and 3%, respectively, when they are heated to 300 K. These high-spin populations are calculated by taking $\mu_{eff} = 5.1\mu_B$ for a high-spin complex and $\mu_{eff} = 0.45\mu_B$ for the low-spin complex. When complex **1** is heated above ~190 K, the high-spin population increases relatively rapidly to a value of 82% at 270 K, above which there is little if any change in the high-spin population. There is 18% of residual low-spin complexes which do not convert readily. Thus, in the series of complexes **1–4**, addition of methyl substituents monotonically leads to a stabilization of the high-spin state relative to the low-spin state. As noted before,[6] this is contrary to what would be expected from the electron-donating effects of methyl group, but probably reflects increasing steric bulk upon adding methyl substituents.

Complex **1** was further characterized by variable-temperature ^{57}Fe Mössbauer spectroscopic and powder X-ray diffraction data. The temperature dependence of the Mössbauer spectrum is illustrated in Figure 2; fitting parameters are given in Table I. In the 30–180 K range only a low-spin quadrupole-split doublet is

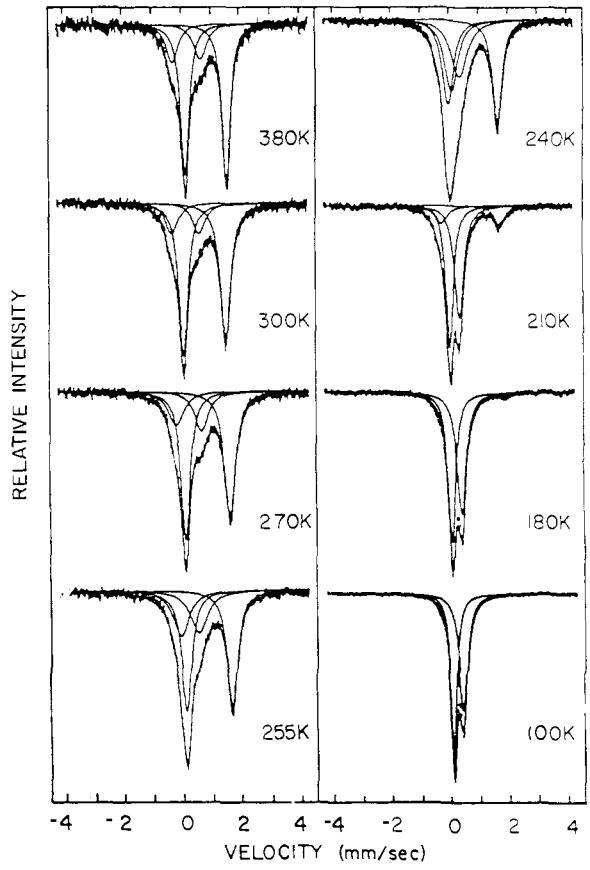

Figure 2. Variable-temperature ^{57}Fe Mössbauer spectra for [Fe(6-Me-py)$_3$tren](ClO$_4$)$_2$ (**1**).

seen. At temperatures above 210 K a high-spin quadrupole-split doublet grows in at the expense of the low-spin doublet. The fraction of the high-spin doublet does not increase above ~270 K. There is ~25% of a residual low-spin fraction above ~270 K which does not convert to high spin. This is in agreement with the residual low-spin fraction indicated by the susceptibility data. The presence of residual low-spin complexes in the sample of a spin-crossover complex has been noted before[9] and has been attributed to the presence of defects which affect the nucleation and growth mechanism.

Variable-temperature (70–340 K) Mössbauer spectra for complex **2** were reported in our previous paper.[1] As the sample temperature is increased, a high-spin doublet first appears at ~250 K, and by ~340 K the Mössbuaer spectrum indicates ~26% high-spin fraction. This is in agreement with the magnetic susceptibility data for this complex.

Spin-Crossover Behavior in Solution. Complexes **1–4** can be dissolved in polar solvents such as CH_2Cl_2, CH_3CN, CH_3OH, CH_3COCH_3, CH_3CH_2OH, and H_2O. In a particular solvent, these complexes exhibit differing amounts of high-spin populations at room temperature. Room-temperature electronic absorption spectra are shown in Figure 3 for complexes **1–4** in acetone. Variable-temperature (200–300 K) UV–vis spectra for acetone solutions show that complex **1** is totally high-spin, whereas complex **4** is totally low-spin. Each spectrum appears to consist of three bands; band positions and molar extinction coefficients are given in Table II. The high-spin complex **1** has much smaller extinction coefficients than those for the low-spin complex **4**. For the low-spin complex, the metal-to-ligand charge-transfer (MLCT) band is located at 553 nm with a shoulder at 510 nm, and the ligand-to-metal charge-transfer (LMCT) band is located at ~360 nm. The MLCT and LMCT bands for the high-spin complex are located at 484 and 330 nm, respectively. The π^* orbitals of the

(9) (a) Haddad, M. S.; Lynch, M. W.; Federer, W. D.; Hendrickson, D. N. *Inorg. Chem.* **1981**, *20*, 123. (b) Haddad, M. S.; Federer, W. D.; Lynch, M. W.; Hendrickson, D. N. *Ibid.* **1981**, *20*, 131.

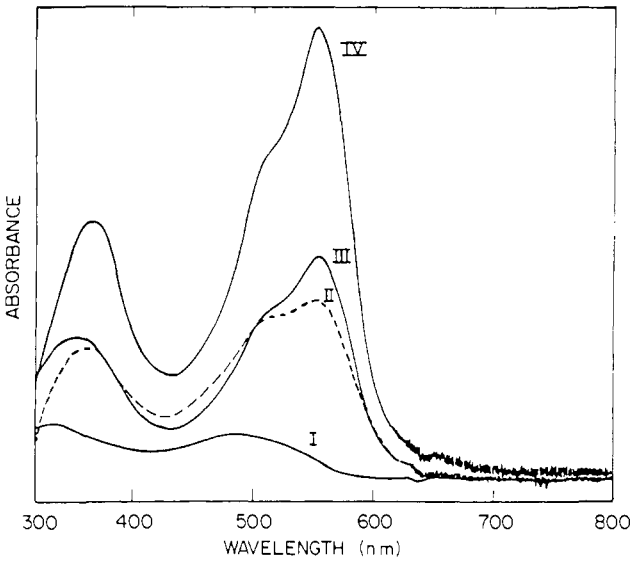

Figure 3. UV–vis electronic absorption spectra for $\sim 5 \times 10^{-4}$ M acetone solutions of I, complex **1**; II, complex, **2**; III, complex **3**; and IV, complex **4**.

Table II. Electronic Absorption Bands and Absorption Coefficients for Complexes **1**, **2**, **3**, and **4**

complex		band I	band II	band III
		Acetone[a]		
1	position[b]	484		330
	coefficient[c]	1500		2400
2	position	553	510[d]	352
	coefficient	7200		5800
3	position	554	510	361
	coefficient	9400		6500
4	position	555	512	368
	coefficient	20000		11200
		Vycor[e]		
2	position	553	510	340
3	position	553	509	348
4	position	555	510	356

[a] In acetone solution at a concentration of 2×10^{-4} M. [b] Band positions in nm. [c] Molar absorption coefficients in M^{-1} dm. [d] As a shoulder of band I. [e] Absorbed into pores of Vycor thirsty glass.

pyridine moieties are most probably involved in these charge-transfer transitions.

Complexes **2** and **3** each exist as a mixture of high-spin and low-spin complexes in acetone. Band positions and extinction coefficients are given in Table II. If it is assumed that the low-spin MLCT bands of complexes **2** and **3** have the same *molar* extinction coefficient at 553 nm as that of the totally low-spin complex **4**, then the high-spin fractions of complexes **2** and **3** in acetone at room temperature can be estimated as 46 and 37%, respectively. The temperature dependence of the absorption spectrum of complex **2** in CH_3CN is shown in Figure 4. As the temperature is decreased, the bands increase in intensity, which reflects an increase in the low-spin fraction.

In the course of examining various media for laser-flash photolysis, Vycor glass was tried. As deduced from variable-temperature UV–vis spectra, it was interesting to find that complexes **2**, **3**, and **4** dissolved in acetone and sorbed into the pores of Vycor glass are totally in their low-spin states. Furthermore, complex **1** is *not* sorbed into the pores of Vycor glass, apparently because the high-spin complex **1** molecules are too large to access the pores of the glass. In the case of complexes **2** and **3** there must be some specific interaction with the walls of the pore or tighter ion pairing, for they are low-spin in the glass pores, but are a mixture of spin states in neat acetone.

Laser-Flash Photolysis of Complexes 1–4 in Acetone: Effect of Zero-Point Energy Difference. As in our previous study[1] of complex **2** doped in polystryene sulfonate (PSS), the frequency-

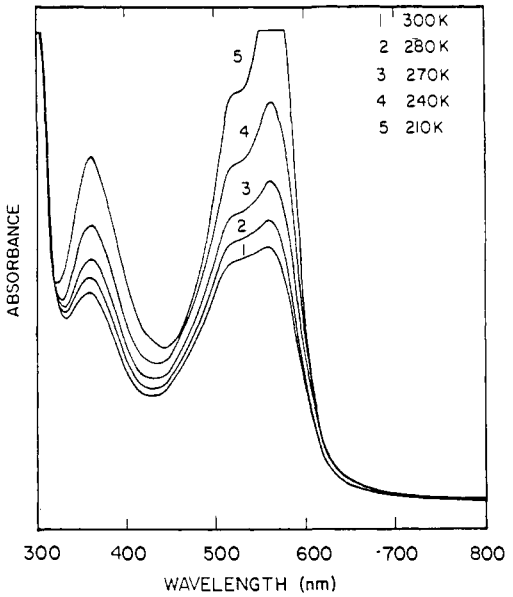

Figure 4. Temperature dependence of the electronic absorption spectrum of a CH_3CN solution of $[Fe(6\text{-}Me\text{-}py)_2(py)tren](ClO_4)_2$, complex **2**.

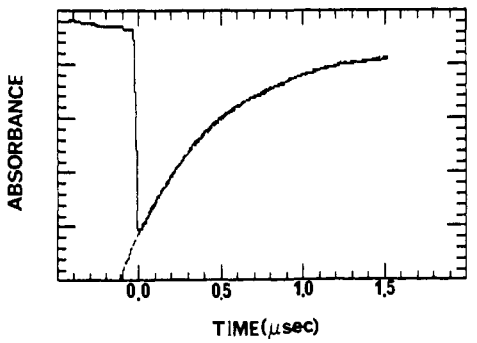

Figure 5. Typical single-pulse transient profile detected at 560 nm for a 0.0539 mM solution of $[Fe(py)_3tren](ClO_4)_2$ (**4**) in acetone at room temperature.

doubled (532 nm) pulse of a Nd/YAG laser is used to excite a low-spin Fe^{II} complex from its $^1A_1$ ground state to the ^{1}MLCT excited state. Some complexes intersystem cross rapidly via triplet states to the $^5T_2$ high-spin state. The relaxation of these $^5T_2$ complexes is monitored after the 35-ns laser pulse by detecting a change in the optical density at some wavelength. Since the high-spin Fe^{II} complexes have only very weak bands in the visible region, changes in the optical density reflect a bleaching and repopulation of the low-spin complexes. The maximum of the MLCT band for the low-spin complexes is located at 560 nm with $\epsilon = 10^4$ M^{-1} cm^{-1}, and it was at this wavelength that the relaxation was monitored. A typical single-pulse transient profile detected at 560 nm for a 0.0539 mM solution of complex **4** in acetone is shown in Figure 5. The dashed line results from a least-squares fit of the data to a single exponential decay of the following form:

$$\Delta A(t) = (\Delta A_0)e^{-t/\tau} \quad (1)$$

$\Delta A(t)$ is the difference between the absorption intensity at 560 nm at time t with that at infinite time (zero time is when the laser is fired). ΔA_0 represents the amplitude of the absorption change generated initially by the laser pulse, and τ is the relaxation time (rate = $k = 1/\tau$). All transient profiles obtained in this study could be fit to the single exponential function in eq 1.

Before the data for the series of complexes **1–4** are discussed, two points should be made. First, the spin-state interconversion rate is *not* influenced by the presence of O_2 in the solution. For example, the relaxation times for complex **2** in degassed acetone and in air-saturated acetone have been measured to be 89 (7) and 93 (7) ns, respectively. Second, we have clearly established that the decrease in absorption at 560 nm in the transient profile

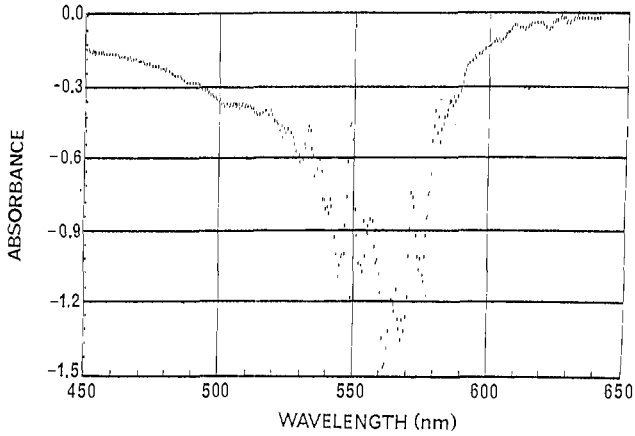

Figure 6. Change in the optical density as detected by a fast optical multichannel analyzer 50 ns after the laser pulse for a 0.25 mM acetone solution of complex **4** at room temperature.

Table III. Spin-State Interconversion Relaxation Rate Constants for Complexes **2**, **3**, and **4** in Acetone[a]

	k ($\times 10^{-7}$ s^{-1})[b]		
T (K)	complex **2**	complex **3**	complex **4**
300	1.08	1.26	1.05
290		0.84	0.932
280	0.697	0.968	0.892
270		0.782	0.827
260	0.527	0.656	0.768
250	0.403	0.558	0.640
240	0.374	0.486	0.552
230	0.278	0.391	0.427
220	0.174	0.311	0.393
210	0.133	0.191	0.319
200	0.101	0.162	0.240
190	0.0621	0.091	0.183
180	0.0378		0.130
E, (cm^{-1})[c]	1029 ± 19	870 ± 15	648 ± 12

[a] Solution concentration at 5×10^{-4} M. [b] Rate constant evaluated as $k = 1/\tau$, where τ is the relaxation time. [c] Apparent Arrhenius activation energy.

recorded following the laser pulse is due to low-spin complexes converting to high-spin complexes ("bleaching") and then relaxing back to the ground low-spin state. A Princeton Instruments Model IRY-512G-V fast optical multichannel analyzer (OMA) was used to observe the absorption spectrum at a variety of times after the laser pulse. In Figure 6 is shown an OMA spectrum for a delay time of 50 ns after the laser pulse for a 0.25 mM acetone solution of complex **4** at room temperature. The change in absorbance is plotted as a function of wavelength. It can be seen that there is a large decrease in absorbance at ~560 nm at this time delay. This is consistent with the occurrence of low-spin bleaching after laser excitation.

Relaxation rates were determined for $\sim 5 \times 10^{-4}$ M acetone solutions of complexes **2**–**4** in the temperature range of 180–300 K. As can be seen in Figure 7, for each of these three complexes a plot of ln k versus $1/T$ gives a straight line. As summarized in Table III, the slopes of the three Arrhenius-type lines in Figure 7 are 648 (12), 870 (15), and 1029 (19) cm^{-1} for complexes **4**, **3**, and **2**, respectively. These apparent activation energies can be discussed with reference to the simplified one-dimensional potential-energy diagram for a spin-crossover complex (see Figure 8). The potential energy of the complex is plotted as a function of the generalized vibrational normal coordinate involved in the spin-state interconversion. The symmetric metal–ligand stretching mode is probably the most important one involved, although other normal coordinate vibrations involving angular deformations could also be important. The high-spin (HS) $^5T_2$ and low-spin (LS) $^1A_1$ states are involved in a second-order spin–orbit interaction via the intermediacy of triplet states. The magnitude of the resonance energy, E_{res}, reflects the magnitude of this second-order

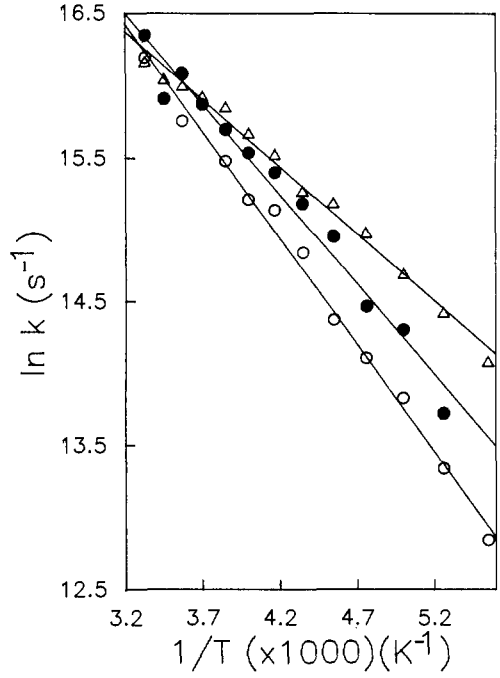

Figure 7. Plots of the natural logarithm of the spin-state interconversion relaxation rate versus inverse temperature for $\sim 5 \times 10^{-4}$ M acetone solutions of (△) [Fe(6-Me-py)$_2$(py)tren](ClO$_4$)$_2$ (**2**), (●) [Fe(6-Me-py)(py)$_2$tren](ClO$_4$)$_2$ (**3**), and (○) [Fe(py)$_3$tren](ClO$_4$)$_2$ (**4**).

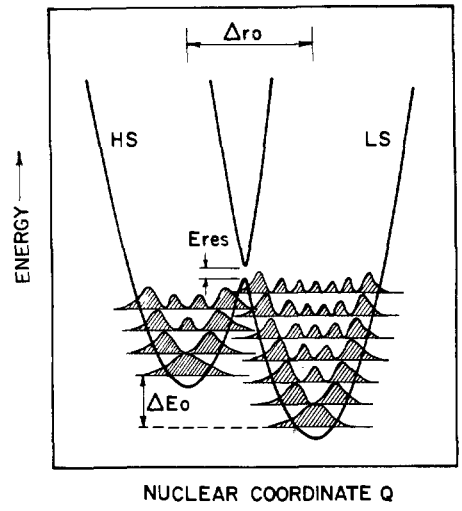

Figure 8. Simplified one-dimensional potential-energy diagram for a Fe^{II} spin-crossover complex. Vibrational levels and associated probability functions corresponding to only one mode, perhaps the symmetric metal–ligand stretching mode, are shown.

spin–orbit interaction. The rate of spin-state interconversion depends on three main factors: the value of E_{res}; the dimensional change Δr_0; and the difference in the zero-point energies, ΔE_0, between the low- and high-spin states.

In the previous section it was established that complex **4** is totally low-spin in acetone and that ΔE_0 decreases in the series **4** > **3** > **2**. In a simple view is could be assumed the above apparent activation energies reflect the energy diference between the zero-point energy level of the $^5T_2$ state and the energy of the barrier. If Δr_0 is assumed to be constant throughout the series, then qualitatively it is understandable why complex **4** with the largest ΔE_0 value exhibits the smallest apparent activation energy. As ΔE_0 becomes smaller the barrier for thermally activating a $^5T_2$ complex to convert to the $^1A_1$ ground state increases.

Solvent Depencence of Spin-State Interconversion Relaxation Rate for Complex 2. Solutions of complex **2** in acetone, acetonitrile, methanol, dichloromethane, and a 2:1 mixture of toluene and acetonitrile were studied with the laser-flash photolysis

Table IV. Spin-State Interconversion Relaxation Rate Constants for $[Fe(6\text{-Me-py})_2(py)tren](ClO_4)_2$ (**2**) in Various Solvents[a]

	k ($\times 10^{-7}$ s^{-1})[b]			
T (K)	aceto-nitrile	dichloro-methane	methanol	toluene/ acetonitrile (2:1)
300			1.060	1.250
295	1.50	0.835		
290			0.752	1.031
280	0.576	0.680	0.701	0.853
270	0.532	0.527	0.638	0.678
260	0.343	0.439	0.484	0.513
250	0.293	0.378	0.410	0.380
240	0.222	0.312	0.371	0.260
230	0.137	0.166	0.296	0.212
220		0.131	0.161	0.169
210		0.0883	0.145	0.0975
200		0.0709	0.0898	0.0785
190		0.0369	0.0428	
180				
E, (cm^{-1})[c]	1310 ± 34	1170 ± 23	1080 ± 24	1010 ± 20

[a] All solution concentrations were 5×10^{-4} M. [b] Rate constant evaluated as $k = 1/\tau$, where τ is the relaxation time. [c] Apparent Arrhenius activation energy.

technique. In each case the concentration of complex **2** was ~5 $\times 10^{-4}$ M. The temperature dependence of the $^5T_2 \rightarrow {}^1A_1$ relaxation time was measured for each solvent from room temperature down to a temperature above the freezing point. Relaxation rate versus temperature data for all five solvent media are collected in Tables III and IV. In the case of each solvent a plot of ln k versus $1/T$ is linear. Apparent activation parameters obtained by fitting the ln k versus $1/T$ data for each solvent are given in Table IV. It is interesting that the slopes of the ln k versus $1/T$ plots for complex **2** vary from 998 (19) cm^{-1} for acetone to 1310 (34) cm^{-1} for acetonitrile. It should be pointed out that the observed Arrhenius behavior, i.e., linear ln k versus $1/T$ plots, does not necessarily indicate that thermal activation over the potential-energy barrier shown in Figure 8 is the mechanism for spin-state interconversion.[10] As we discussed in our previous paper,[1] spin-state interconversion via a tunneling mechanism could well also give a linear ln k versus $1/T$ plot.

The pronounced solvent dependence of the activation energy for the spin-state interconversion of complex **2** reflects in some way an important role for the solvent in the spin-state interconversion dynamics. The microscopic mechanism of how solvent molecules participate in this process is not clearly known. Several possibilities can be briefly discussed.

In the case of complex **2**, obviously the $[Fe^{II}(6\text{-Me-py})_2(py)tren]^{2+}$ cation exists in some solvated form in solution. The solvation energy could be different for te $^5T_2$ and $^1A_1$ states, and this difference may vary from one solvent to another.[11,12] This difference in the solvation energy between the two states will add to the zero-point energy difference, ΔE_0. In this way, ΔE_0 may be solvent dependent. However, for complex **2** in the five solvents investigated there does not seem to be any obvious simple correlation of this type. Acetone and methanol are perhaps the better solvating media and they do exhibit two of the smaller activation energies, but the activation energy observed for the 2:1 toluene/CH_3CN mixture is less than for methanol. Futhermore, there is no simple correlation with dielectric constants: CH_3CN (37.5), CH_3OH (32.6), CH_3COCH_3 (20.7), and CH_2Cl_2 (9.08). Moreover, there is a possibility that in some of these solvents appreciable ion pairing or aggregation occurs. This possibility is investigated further below.

Another possible origin for the solvent dependence is that the electron-vibrational coupling[13] which is present in these spin-crossover complexes leads to an interaction between the electronic wave function and the solvent vibrational modes. This solvent modulation of the electron–phonon interaction could be mediated through interactions between the intramolecular and solvent vibrational modes. As a consequence, the solvent vibrational modes can modify the potential-energy surfaces (Figure 8) and in turn modify the spin-state interconversion dynamics.

Table V. Spin-State Interconversion Relaxation Rate Constants for $[Fe(py)_3tren](ClO_4)_2$ at Four Different Concentrations in Acetone

	k ($\times 10^{-7}$ s^{-1})[a]			
T (K)	0.0539 mM	0.105 mM	0.272 mM	0.500 mM
180				0.13
185	0.083	0.0948	0.1222	
190	0.0943	0.1227	0.1486	0.183
195	0.1024	0.1415	0.1594	
200	0.1408	0.164	0.1755	0.24
205	0.1811	0.2014	0.2005	
210	0.2361	0.2205		0.319
215		0.2948	0.2339	
220	0.3047	0.331	0.2789	0.393
225		0.4043		
230	0.3438	0.4636	0.33	0.427
240	0.4348		0.4691	0.552
250	0.5542	0.6506	0.6261	0.64
260	0.8283	0.79	0.7473	0.768
270	1.191	1.319	0.9088	0.827
280	1.471		1.078	0.892
290				0.932
300				1.05
E (cm^{-1})[b]	1072 (28)	1007 (20)	834 (15)	649 (12)
ln A (s^{-1})[c]	21.88 (20)	21.59 (21)	20.42 (33)	19.36 (23)

[a] Rate constant evaluated as $k = 1/\tau$, where τ is the relaxation time. [b] Apparent Arrhenius activation energy. [c] Natural logarithm of preexponential (i.e., intercept) from Arrhenius plot.

Jortner et al.[14] described the spin-crossover phenomenon in solution in terms of a radiationless multiphonon process occurring between two distinct (zero order) spin states ($^5T_2$ and $^1A_1$) which are characterized by different nuclear equilibrium configurations separated by a potential-energy barrier which is large relative to the thermal energy kT. They assumed that the spin-state interconversion is nonadiabatic and employed the "Golden Rule" with total wave functions as products of an electronic wave function and a nuclear wave function, both for the internal modes of the complex as well as the solvent modes, to derive an expression for the rate of spin-state interconversion. This simply means that not only can the $^5T_2$ complex relax to the $^1A_1$ ground state by tunneling from each of the vibrational levels (overtones of one active intramolecular mode), but there is about each of the pictured vibrational levels a distribution of vibrational levels associated with the solvent structure. The complex can tunnel via many vibrational levels. Because the nature of the solvent structure determines the distribution of solvent modes, there can be a solvent dependence in the apparent activation energy. In this case the "activation" energy would reflect differences in rates of tunneling.

Yet another possible source of the solvent dependence of the activation energy could originate in having a vibrational level relaxation rate which is comparable to the spin-state interconversion rate. It is well known[15] that vibrational relaxation can be dramatically influenced by the solvent.

Concentration Dependence of Spin-State Interconversion Rate for Complex 4. In an effort to try to understand the origin of the solvent dependence of the $^5T_2 \rightarrow {}^1A_1$ relaxation, we studied the concentration dependence of this relaxation rate. Complex **4** was selected because it shows the greatest low-spin population in solution in the series, and, therefore, optical density changes after

(10) See, for example: DeVault, D. *Quantum-Mechanical Tunnelling* in *Biological Systems*; Cambridge University Press: Cambridge, 1984.
(11) Buhks, E.; Bixon, M.; Jortner, J.; Navon, G. *Inorg. Chem.* **1979**, *18*, 2014.
(12) Zhu, T.; Su, C.; Schaeper, D.; Lamke, B.; Wilson, L. *Inorg. Chem.* **1984**, *23*, 4345.
(13) (a) Sorai, M.; Seki, S. *J. Phys. Chem. Solids* **1974**, *35*, 555. (b) Liehr, A. *Prog. Inorg. Chem.* **1962**, *3*, 281.
(14) Buhks, E.; Navon, G.; Bixon, M.; Jortner, J. *J. Am. Chem. Soc.* **1980**, *102*, 2918.
(15) Rothschild, W. G. *Dynamics of Molecular Liquids*; John Wiley & Sons: New York, 1984.

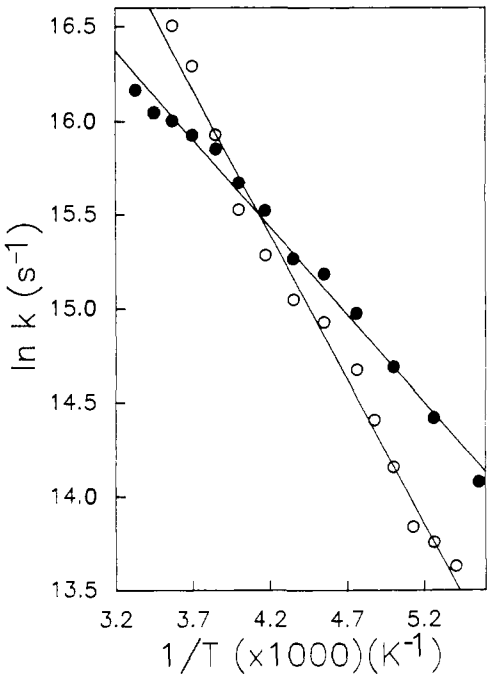

Figure 9. Plots of the natural logarithm of the spin-state interconversion relaxation rate versus inverse temperature for two different concentration acetone solutions of $[Fe(py)_3tren](ClO_4)_2$ (**4**): (○) 0.0539 mM, (●) 0.500 mM.

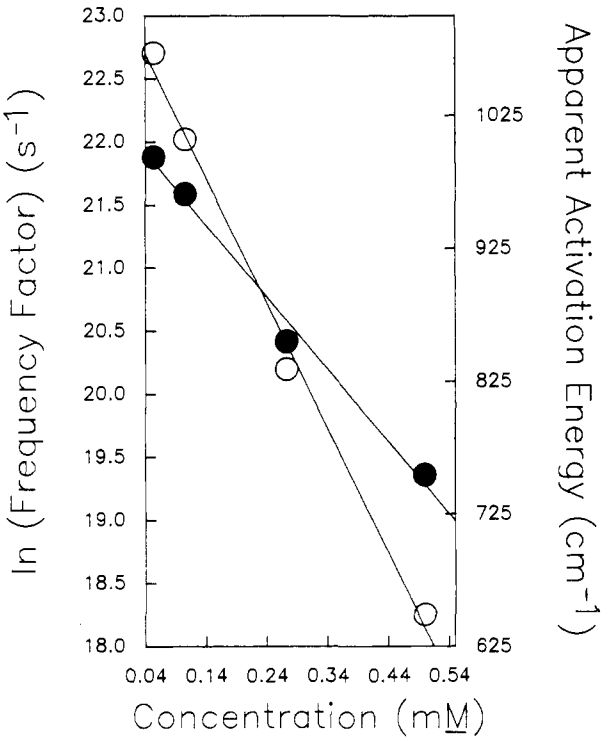

Figure 10. Plots of the Arrhenius activation energy (○) versus concentration and natural logarithm of Arrhenius preexponential factor (●) versus concentration for acetone solutions of $[Fe(py)_3tren](ClO_4)_2$ (**4**).

a laser pulse are greater for this complex.

Complex **4** was studied at the concentrations of 0.0539, 0.105, 0.272, and 0.500 mM in acetone. Variable-temperature relaxation rates are given in Table V for these four solutions. It was quite surprising to find that a variation of the concentration of complex **4** in acetone in the range of $\sim 5 \times 10^{-5}$ to $\sim 5 \times 10^{-4}$ M has a pronounced effect on the relaxation rate. At each concentration a linear Arrhenius plot was found. In Figure 9 are shown the ln k versus $1/T$ plots for the two limiting concentrations. At a concentration of 0.500 mM the activation energy is found by

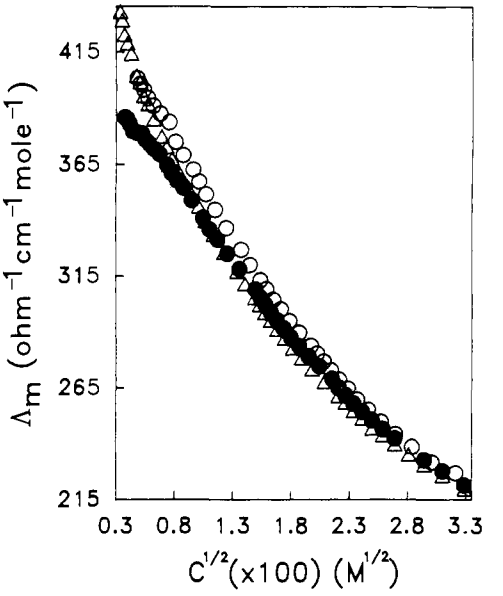

Figure 11. Plots of the molar conductivity versus the square root of the concentration for acetone solutions of complexes **2** (○), **3** (●), and **4** (△).

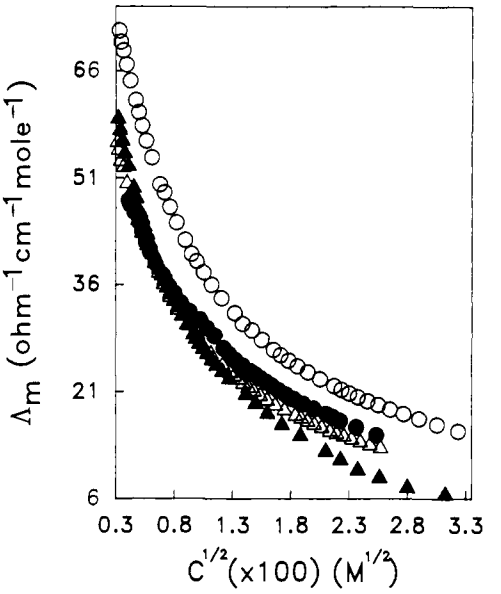

Figure 12. Plots of the molar conductivity vs the square root of the concentration for CH_2Cl_2 solutions of complexes **1** (○), **2** (●), **3** (△), and **4** (▲).

least-squares fitting (see line in Figure 9) to be 649 cm^{-1}, whereas at 0.0539 mM the activation energy has increased by ~65% to a value of 1072 cm^{-1}. The preexponential (intercept of ln k versus $1/T$ plot) also changes from 19.4 to 21.9 s^{-1}, respectively. Perhaps as surprising as the change in the activation energy is the fact, as illustrated in Figure 10, that both the activation energy and preexponential term vary linearly with concentration.

The origin of this interesting and appreciable concentration dependence of spin-state interconversion relaxation rate was elucidated by measuring the electrical conductivity of solutions. The dynamical theory of concentrated electrolyte solutions is complicated and in some cases controversial.[16] However, the concept of an ion pair is generally understood. Some of the ions in the electrolyte soup can be considered bound together and thus do not contribute as charge carriers to the overall conductance of the solution.[17] In the present case the 2+ charged Fe^{II} cation

(16) (a) Wolynes, P. G. *Annu. Rev. Phys. Chem.* **1980**, *31*, 345. (b) Dogonadze, R.; Kälman, E.; Kornyshev, A. A.; Ulstrup, J., Eds., *The Chemical Physics of Solvation*, Vols. A, B, and C; Elsevier: Amsterdam (1985, 1986, 1986).

could be associated with two ClO_4^- anions.

Molar conductivities were determined at 25 °C for acetone solutions of complexes **2**, **3**, and **4** in the concentration range of $\sim 10^{-3}$ to $\sim 10^{-5}$ M. Figure 11 gives for each of the three complexes at 25 °C a plot of molar conductivity in acetone versus $(C)^{1/2}$, where C is the concentration of the complex. In Figure 12 are shown plots of molar conductivity at 25 °C in CH_2Cl_2 versus $(C)^{1/2}$ for complexes **1–4**. It is clear from these two figures that even in acetone which has a dielectric constant of 20.7 at 25 °C ion pairing is present not only at $\sim 10^{-3}$ M, but also persists down to $\sim 10^{-5}$ M. If there was no ion pairing present in a solution, a plot of molar conductivity versus $(C)^{1/2}$ should give a straight line. For solutions of a 1:2 electrolyte, such as we have for these Fe^{II} complexes, it is not possible to evaluate equilibrium constants for the ion-pairing equilibria (actually there are probably present in each solution multiple equilibra associated with different levels of ion aggregation). One final point can be made about the solution conductivity data. Examination of the data in Figures 11 and 12 show that for a given solvent there is an increase in conductivity in the order complex **1** > **2** > **3** > **4** at a given concentration. This implies that the ion-pairing effects are greatest for the low-spin complex **4** and least for the high-spin complex **1**.

Regardless of the details of any analysis of the solution conductivities, one main conclusion may be drawn. The concentration dependence of the activation energy for spin-state interconversion of complex **4** in the $\sim 5 \times 10^{-5}$ to $\sim 5 \times 10^{-4}$ M range in acetone probably reflects a variable degree of ion aggregation.

Theoretical Modeling of the Concentration Dependence of Spin-State Interconversion Rate. A fitting of the $^5T_2 \rightarrow {}^1A_1$ relaxation rate data to theoretical models can give insight about the origin(s) of the observed concentration dependence of the activation energy for complex **4** in acetone.

Hopfield[18] developed an equation for the rate of electron tunneling between two fixed sites based on Förster's electron-transfer theory. A molecule is interconverting between two states which are only weakly interacting with each other. Hopfield's equation for the rate, w_{ab}, of tunneling between states a and b, each with one vibrational mode active, is

$$w_{ab} = \frac{2\pi}{\hbar}|T_{ab}|^2\left(\frac{1}{2\pi\sigma^2}\right)^{1/2} \exp[-(E_a - E_b - \Delta)^2/2\sigma^2] \quad (2)$$

where

$$\sigma^2 = \left(\frac{k_a X_a^2}{2}\right)(k_B T_a) \coth\left(\frac{T_a}{2T}\right) \quad (3)$$

and

$$\Delta = \tfrac{1}{2}k_a X_a^2 + \tfrac{1}{2}k_b X_b^2 \quad (4)$$

In these equations, T_{ab} is the tunneling matrix element (i.e., electronic coupling), k_B is Boltzmann's constant, T_a ($=\hbar\omega_a/k_B$) is the temperature equivalent of the quantum of the active vibrational mode which is assumed to be the same in the states a and b, $(E_a - E_b)$ is the difference in zero-point energies of the two states, and $1/2\ k_a X_a^2$ reflects the reorganization energy for converting from state a to state b along the electronic potential energy curve of state a.

In order to limit the number of parameters employed in least-square fitting the relaxation rate data to eq 2, it was decided to hold T_a (T_b) at a constant value. This left three parameters: T_{ab}, Δ, and $E_a - E_b = \Delta E_0$. The relaxation rate data sets for each of the four different concentrations of complex **4** were fit to eq 2 to give the parameters listed in Table VI. In order to check the effect of variations in the vibrational quantum, T_a values of 200, 300, and 400 K were employed as constants in the fits. The trends in T_{ab}, Δ, and ΔE_0 are the same for all three settings of T_a. The specific results with T_a held constant at 300 K (i.e., $\hbar\omega$ = 208 cm^{-1}) are representative. As can be seen in Table VI, there is little variation in the reorganization parameter Δ as the concentration of complex **4** is increased from 0.0539 to 0.500 mM. With T_a = 300 K the tunneling matrix element T_{ab} decreases by a factor of ~8 from 14.5 to 1.8 cm^{-1} as the concentration of complex **4** is increased from 0.0539 to 0.500 mM. Since the rate w_{ab} depends on $|T_{ab}|^2$, this decrease in T_{ab} leads to a ~64-fold decrease in rate of interconversion as the concentration is increased. However, the largest change in the three parameters is found for the zero-point energy difference ΔE_0, which with T_a = 300 K increases by a factor of ~211 from 8.8 to 1855 cm^{-1} as the concentration is increased from 0.0539 to 0.500 mM.

Table VI. Parameters Resulting from Least-Squares Fitting of Relaxation Rate Data for Complex **4** in Acetone to Hopfield's Model

parameter	conc of complex **4** (mM) 0.0539	0.105	0.272	0.500
	$T_a = T_b$ = 200 K (fixed)			
T_{ab} (cm^{-1})	7.4	5.2	3.1	1.2
Δ (eV)	0.72	0.76	0.81	0.68
ΔE_0 (cm^{-1})	34	483	1065	1266
	$T_a = T_b$ = 300 K (fixed)			
T_{ab} (cm^{-1})	14.5	9.7	5.2	1.8
Δ (eV)	0.88	0.88	0.91	0.88
ΔE_0 (cm^{-1})	8.8	340	927	1855
	$T_a = T_b$ = 400 K (fixed)			
T_{ab} (cm^{-1})	40.8	26.7	11.0	2.8
Δ (eV)	1.15	1.15	0.97	0.91
ΔE_0 (cm^{-1})	21.4	438	302	1309

Before the possible meanings of these parameters are discussed, it is important to comment on the Hopfield model-fitting parameters, which were obtained[1] by fitting the 4.2–300 K relaxation data for complex **2** in polystyrene sulfonate (PSS). The previously reported[1] parameters of T_{ab} = 52.8 cm^{-1}, T_a = 283 K, and Δ = 0.76 eV (ΔE_0 taken as 400 cm^{-1}) are in error because we inadvertently erred in multiplying the rate constant values given in Table II of ref 1 by $\hbar$ to get $\hbar k$ values used in the fitting. When the correct values of $\hbar k$ are used for the data for complex **2** dispersed in PSS, we find T_{ab} = 6.4 cm^{-1}, $T_a = T_b$ = 287 K, and Δ = 0.79 eV with ΔE_0 fixed at 400 cm^{-1}. Thus, fitting the 4.2–300 K data for complex **2** in PSS also gives the same magnitude of parameters as we get from fitting the solution data.

The next obvious question is why the tunneling matrix element T_{ab} is so small in all of these fittings. In the case of a Fe^{II} spin-crossover complex, the parameter T_{ab} gauges the magnitude of the interaction between the $^1A_1$ and $^5T_2$ states. It is equivalent to E_{res} in Figure 9. The $^1A_1$ and $^5T_2$ states interact via a second-order spin–orbit interaction through the intermediacy of triplet states such as the $^3T_1$ state. That is, in the Hamiltonian matrix involving the $^1A_1$, $^5T_2$, and $^3T_1$ states, there are off-diagonal matrix terms between the $^1A_1$ and $^3T_1$ states and between the $^5T_2$ and $^3T_1$ states. The presence of these two types of off-diagonal matrix elements leads to an interaction between the $^1A_1$ and $^5T_2$ states. If only the *electronic* wave functions are used, T_{ab} would be expected[14,19] to be of the order of magnitude 50–200 cm^{-1}. However, vibronic interactions could well considerably reduce the magnitude of T_{ab}. Strong coupling of the $^1A_1$ and $^5T_2$ electronic coordinates to vibrational wave functions, i.e., a breakdown of the Born–Oppenheimer approximation, leads to appreciable vibronic interactions. The reduction of physical quantities of electronic origin is one of the important consequences of vibronic interactions.[20] The Ham effect[21] is well known in EPR spectroscopy, where vibronic interactions dramatically affect observables such as g values.

In the case of the Fe^{II} spin-crossover complexes, the off-diagonal matrix element (electronic in origin) due to spin–orbit interaction between the $^1A_1$ and $^3T_1$ state, for example, is to be multiplied

(17) Geary, W. J. *Coord. Chem. Rev.* **1971**, *81*, 122.
(18) Hopfield, J. L. *Proc. Natl. Acad. Sci. U.S.A.* **1974**, *71*, 3640.
(19) Sutin, N. *Acc. Chem. Res.* **1982**, *15*, 275.
(20) Bersuker, I. B. *The Jahn-Teller Effect and Vibronic Interactions in Modern Chemistry*; Plenum Press: New York, 1984.
(21) Ham, F. S. In *Electron Paramagnetic Resonance*; Geschwind, S., Ed.; Plenum Press: New York, 1972; Chapter 1.

by an integral of two vibrational wave functions, one for the $^1A_1$ and the other for the $^3T_1$ state. This vibrational overlap integral is less than unity and it reduces the value of the off-diagonal matrix element. This reduces T_{ab}. Vibronic interactions which lead to reductions by one to two orders of magnitude in electronic terms are well documented.[20,21] Thus, it is not at all impossible to have tunneling matrix elements (T_{ab}) as small as 1–10 cm^{-1}.

Before the above trends in Hopfield model-fitting parameters as a function of concentration are discussed with an eye to the physical origins, the results from a second theoretical model are examined. Jortner et al.[14] described the spin-crossover phenomenon in solution in terms of a radiationless multiphonon process occurring between two distinct spin states which are characterized by different nuclear equilibrium configurations separated by a potential-energy barrier which is large relative to the thermal energy k_BT. They assumed that the spin-state interconversion is nonadiabatic and employed the "Golden Rule". The total wave functions were taken as products of an electronic wave function and nuclear wave function both for the internal modes of the complex as well as the solvent modes. An expression for the rate of spin-state interconversion was found to be

$$k = (2\pi/\hbar)g_f|V|^2G \tag{5}$$

The paremeter g_f is the degeneracy change in converting from the low-spin to the high-spin state: i.e., $g_f = g_{HS}/g_{LS} = 5/1 = 5$. $|V|$ gauges the magnitude of the coupling between the $^1A_1$ and $^5T_2$ states (analogous to T_{ab}) caused by a spin–orbit interaction. The thermally averaged Franck–Condon vibrational overlap factor G accounts for the contribution of the solvent and metal–ligand vibrational modes. In order to get an analytical expression for G, a relatively simple model of the vibrational mode was assumed. The solvent was represented by very low frequency oscillators, and it was assumed that only one metal–ligand vibrational mode (same frequency in both states) coupled to the spin-state interconversion to derive an expression for G. The electronic spin–orbit coupling was taken as:

$$V = -3\sqrt{2}\xi^2\left(\frac{1}{\Delta E_1} + \frac{1}{\Delta E_2}\right) \tag{6}$$

where ξ is the spin–orbit coupling constant, ΔE_1 is the energy difference between the $^3T_1$ and $^1A_1$ states, and ΔE_2 is the energy difference between the $^3T_1$ and $^5T_2$ states. A fit to eq 5 requires the parameters ξ, ΔE_1, ΔE_2, $\hbar\omega$, p, and S. The parameters $\hbar\omega$, p, and S are part of the expression for the vibrational overlap factor G derived by Jortner et al. The one active metal–ligand vibrational mode is characterized by $\hbar\omega$, p ($=\Delta E_0/\hbar w$) is simply the reduced value of the zero-point energy difference, and the coupling parameter S measures the contribution of the change in the metal–ligand vibrational mode

$$S = m\omega(\Delta r_0)^2/2\hbar \tag{7}$$

where m is the reduced mass.

In the fitting of rate data to eq 5 it was elected to hold ΔE_1 and ΔE_2 fixed as 1.05×10^4 and 1.94×10^4 cm^{-1}, respectively. These values were obtained in refitting the *corrected* rate values for complex **2** in PSS, together with the parameters $\xi = 59.6$ cm^{-1}, $\hbar\omega = 312$ cm^{-1}, and $S = 18.3$ with p held fixed at a value of -1. Previously we reported[1] fitting parameters of $\Delta E_1 = 1.05 \times 10^4$ cm^{-1}, $\Delta E_2 = 1..94 \times 10^4$ cm^{-1}, $\xi = 164$ cm^{-1}, $\hbar\omega = 290$ cm^{-1}, and $S = 18.2$ for fitting the data for complex **2** in PSS.

In Table VII are given the parameters resulting from fitting the data for the concentration dependence of the rate to eq 5. In analogy to the procedure used for fitting data to eq 2, we tried several different fittings where $\hbar\omega$ was held fixed at 200, 400, or 600 cm^{-1}. Unfortunately, because the zero-point functionality ($p = \Delta E_0/\hbar\omega$) involves a modified Bessel-type function, we could only employ integer values ($p = -1$, -2, or -3) of p. Thus, for each fit only the coupling parameter S and the spin–orbit parameter ξ were varied with each fixed set of p and $\hbar\omega$ values. Perhaps three observations can be made from the variations in parameters. The coupling parameter S does not vary appreciably as the concentration of complex **4** is increased from 0.0539 to 0.500 mM. Second, the spin–orbit coupling parameter ξ is found to be small compared to $\xi = 400$ cm^{-1} for a gaseous free Fe^{II} ion. A small value for ξ from the fitting to eq 5 is consistent with the small value of the tunneling matrix element T_{ab} obtained by fitting the data to eq 2. Appreciable vibronic interactions account for small values of T_{ab}, or equivalently small values of ξ.

Table VII. Parameters Resultant from Least-Squares Fitting of Relaxation Rate Data for Complex **4** in Acetone to Jortner's Model[a]

	parameters: ξ; S at different conc of complex **4** (mM)			
$\hbar\omega$ (fixed)	0.0539	0.105	0.272	0.500
		$p = -1$ (fixed)		
200	61; 28	55; 26	40; 22	28; 18
400	109; 20	96; 19	64; 17	42; 14
600	300; 22	300; 22	170; 19	88; 15
		$p = -2$ (fixed)		
200	61; 30	55.9; 28	41; 25	30; 20
400	122; 23	108; 22	72; 20	47; 17
600	400; 25	451; 26	248; 23	128; 20
		$p = 0$ (fixed)		
200	60; 26	54; 24	39; 20	28; 16
400	97; 17	85; 16	58; 14	37; 11
600	129; 18	201; 17	115; 14	58; 10

[a] The two energy differences determining the spin–orbit coupling (eq 6) were held constant throughout all fittings as $\Delta E_1 = 1.05 \times 10^4$ cm^{-1} and $\Delta E_2 = 1.94 \times 10^4$ cm^{-1}. The parameters p and $\hbar\omega$ were also held fixed at various values. Tabulated are the fitting parameters ξ and S; see text for definitions of terms.

The third observation which can be made from the fitting parameters in Table VII is that ξ decreases in value as the concentration of complex **4** is increased. This agrees with the fitting to the other model. Unfortunately, information about a variation in the value of ΔE_0 is not easily forthcoming from the fitting to the Jortner model.

Physical Origin of Concentration Dependence of Spin-State Interconversion Rate. It is possible to rationalize the concentration dependence on the $^5T_2 \rightarrow {}^1A_1$ rate in terms of ion-pairing effects. Fitting of the rate data for complex **4** to the Hopfield eq 2 suggests that the zero-point energy difference ΔE_0 (Figure 8) increases as the concentration of complex **4** in acetone is increased from 0.0539 to 0.500 mM. Conductivity data for acetone solutions of complex **4** in this concentration range clearly show that the extent of ion-pairing is increasing from 0.0539 to 0.500 mM. With little ion pairing in a dilute solution the Fe^{II} cation is only surrounded by solvent molecules and ΔE_0 assumes a certain value. It is not unreasonable to propose that as the Fe^{II} cation becomes surrounded by ClO_4^- anions at higher concentration there is an increase in the value of ΔE_0. This is same type of observation we very recently reported[5] for the mixed-valence biferrocenium cation in solution. The energy of the intervalence-transfer electronic absorption band found in the NIR was found to increase in energy as the concenration of biferrocenium triiodide in a solvent was increased. The double-well potential-energy diagram, vibronic interaction, and sensitivity to environment characteristics of spin-crossover and binuclear mixed-valence comlexes are very similar.

An increase in the zero-point energy difference ΔE_0 in response to an increase in concentration of complex **4** in acetone could also explain the observed variation in "activation" energy as a function of concentration. If we accept the view which emerges from the fits to the theoretical models that T_{ab} (E_{res} in Figure 8) is quite small, then these spin-crossover complexes are *not* thermally activated over a potential-energy barrier, but they tunnel from the $^5T_2$ to the $^1A_1$ state. An Arrhenius-like behavior would come then from a Boltzmann distribution of complexes in different vibrational levels of the $^5T_2$ state, where each vibrational level has a different rate of tunneling from the $^5T_2$ to the $^1A_1$ state. When ΔE_0 is large, perhaps due to ion pairing at high concentrations, rates of tunneling from vibrational levels in the $^5T_2$ state to energetically similar vibrational levels in the $^1A_1$ state will be greater than the tunneling rates found for the case where ΔE_0 is smaller.

In the former case the vibrational levels of the $^1A_1$ state which are involved are higher energy levels than in the small ΔE_0 case. The probability distributions for higher energy vibrational levels have "tails" which go further into the potential-energy barrier and facilitate tunneling.

Studies are in progress to investigate the effects on the spin-state interconversion rate of added electrolyte, of added analogous Zn^{II} complex, and of changing the solvent to a higher dielectric solvent than acetone. We are also investigating whether part of the change in apparent Arrhenius activation energy as a function of concentration is not only due to changes in ΔE_0 for a given complex, but may also be due to differences in activation energies to form different-sized aggregates.

Acknowledgment. We are grateful for support from National Institutes of Health Grant HL16352 and discussions with Professor Peter Wolynes and we thank Dr. Bruce S. Brunschwig for pointing out calculational errors in ref 1.

Ultraviolet Photoelectron and ESR Studies of 1,2,4,6-Thiatriazinyl and 1,2,3,5-Dithiadiazolyl Radicals

René T. Boeré, Richard T. Oakley,* Robert W. Reed, and Nicholas P. C. Westwood*

Contribution from the Guelph-Waterloo Centre for Graduate Work in Chemistry, Guelph Campus, Department of Chemistry and Biochemistry, University of Guelph, Guelph, Ontario N1G 2W1, Canada. *Received June 24, 1988*

Abstract: 1,2,4,6-Thiatriazinyl radicals, $[R_2C_2N_3S]^\bullet$, and 1,2,3,5-dithiadiazolyl radicals, $[RCN_2S_2]^\bullet$ (R = CF_3, Cl, Ph), have been generated in the gas phase and studied by He I photoelectron spectroscopy. Thiatriazinyls with R = CF_3, Cl, 4-$MeOC_6H_4$, and 4-$NO_2C_6H_4$ have also been prepared in solution and characterized by ESR spectroscopy. Ionization potential and hyperfine coupling constant data for these radical systems are analyzed in relation to the results of MNDO calculations on their electronic structures; the effects of conjugative interactions between the exocyclic ligand(s) and the heterocyclic ring are more pronounced in the thiatriazinyl system.

Many of the recent developments in heterocyclic thiazene chemistry have been concerned with the generation, energetics of association, and the rearrangements of radical systems.[1] In our work we have focused attention on the properties of 1,2,4,6-thiatriazinyl radicals **1**,[2-4] in particular, the potential use of these

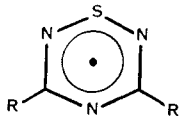

1

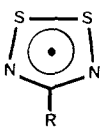

2

and related derivatives in the design of low-dimensional molecular metals.[5] To this end we have been concerned with the dependence of molecular properties, e.g., spin distributions and ionization potentials, on the nature of the 3,5-ligands.[4] Radicals based on the 1,2,3,5-dithiadiazolyl framework **2** have also received considerable attention; derivatives with a variety of R groups have been characterized by ESR spectroscopy,[6] and the solid-state structures of the radical dimers of **2** (R = Ph and CF_3)[6a,7] have been reported. The structure of **2** (R = CF_3) has also been studied in the gas phase by electron diffraction.[6a]

Table I. Ionization Potentials (eV) of **1**, $[R_2C_2N_3S]^\bullet$, and **2**, $[RCN_2S_2]^\bullet$ [a-c]

1, R =			2, R =		
CF_3	Cl	Ph	CF_3	Cl	Ph
(8.6)	(8.18)	(6.81)	(7.94)	(7.73)	(7.10)
9.1	8.57	7.35	8.25	8.00	7.40
11.5	11.0 (sh)	8.9 (sh)	11.1	10.27	8.9
12.2	11.29	9.2	11.65	11.0 (sh)	9.4
12.7	12.22	9.4	12.0	11.33	10.2 (sh)
13.7	12.79	10.9	13.23	11.80	10.6
14.6	13.79 (sh)	11.9	14.5	12.30	11.2
15.3 (sh)	14.06	12.8	15.08	12.69	12.1
15.7	15.44	14.1	15.9	13.41	13.0
	17.2	14.6	16.9	15.04	14.1
				16.5	14.9

[a] Onsets (assumed adiabatics) for the first IPs in parentheses; all other IPs are vertical, or estimated band maxima in the case of broad/unresolved features. [b] First IPs are ±0.04 eV except for **1** (R = CF_3). All other bands are either ±0.06 or ±0.1 eV. [c] (sh) refers to a shoulder on the side of a maximum.

In order to probe more deeply the electronic structures of **1** and **2**, we have turned to the use of UV photoelectron spectroscopy (UPS). In general, the analysis of radicals by UPS has been restricted. Aside from the usual stable open-shell molecules, e.g., O_2, NO, NO_2, most photoelectron studies have focused on extremely short-lived di-, tri-, and tetraatomic radicals,[8] including NS,[9] together with a few assorted organic species, i.e., alkyls,[8,10] nitroxides,[11] benzyl,[12] phenyl,[13] tropyl,[14] and phenoxy.[15] In most

(1) Oakley, R. T. *Prog. Inorg. Chem.* **1988**, *36*, 299.
(2) Hayes, P. J.; Oakley, R. T.; Cordes, A. W.; Pennington, W. T. *J. Am. Chem. Soc.* **1985**, *107*, 1346.
(3) Oakley, R. T.; Reed, R. W.; Cordes, A. W.; Craig, S. L.; Graham, J. B. *J. Am. Chem. Soc.* **1987**, *109*, 7745.
(4) Boerê, R. T.; Cordes, A. W.; Hayes, P. J.; Oakley, R. T.; Reed, R. W.; Pennington, W. T. *Inorg. Chem.* **1986**, *25*, 2445.
(5) Haddon, R. C. *Aust. J. Chem.* **1975**, *28*, 2343.
(6) (a) Höfs, H.-U.; Bats, J. W.; Gleiter, R.; Hartmann, G.; Mews, R.; Eckert-Maksič, M.; Oberhammer, H.; Sheldrick, G. M. *Chem. Ber.* **1985**, *118*, 3781. (b) Markovskii, L. N.; Polumbrik, P. M.; Talanov, V. S.; Shermolovich, Yu. G. *Tetrahedron Lett.* **1982**, *23*, 761. (c) Müller, T. Dissertation, University of Frankfurt, 1979. (d) Fairhurst, S. A.; Johnson, K. M.; Sutcliffe, L. H.; Preston, K. F.; Banister, A. J.; Hauptmann, Z. V.; Passmore, J. *J. Chem. Soc., Dalton Trans.* **1986**, 1465.
(7) Vegas, A.; Pérez-Salazar, A.; Banister, A. J.; Hey, R. G. *J. Chem. Soc., Dalton Trans.* **1980**, 1812.
(8) Dyke, J. M.; Jonathan, N.; Morris, A. *Int. Rev. Phys. Chem.* **1982**, *2*, 3.
(9) Dyke, J. M.; Morris, A.; Trickle, I. R. *J. Chem. Soc., Faraday Trans. 2* **1977**, *73*, 147.
(10) Dearden, D. V.; Beauchamp, J. L. *J. Phys. Chem.* **1985**, *89*, 5359, and references therein.
(11) Morishima, I.; Yoshikawa, K.; Yonezawa, T.; Matsumoto, H.; *Chem. Phys. Lett.* **1972**, *16*, 336.

0002-7863/89/1511-1180$01.50/0